
BrainSymphony: A Transformer-Driven Fusion of fMRI Time Series and Structural Connectivity

Moein Khajehnejad

Turner Institute for Brain and Mental Health,
Monash University, Australia
moein.khajehnejad@monash.edu

Forough Habibollahi

Cortical Labs Pty Ltd,
Melbourne, Australia
forough@corticalabs.com

Adeel Razi

Turner Institute for Brain and Mental Health,
Monash University, Australia
CIFAR Azrieli Global Scholars Program, CIFAR, Toronto, Canada
Wellcome Centre for Human Neuroimaging, UCL, UK
adeel.razi@monash.edu

Abstract

Existing foundation models for neuroimaging are often prohibitively large and data-intensive. We introduce BrainSymphony, a lightweight, parameter-efficient foundation model that achieves state-of-the-art performance while being pre-trained on significantly smaller public datasets. BrainSymphony’s strong multimodal architecture processes functional MRI data through parallel spatial and temporal transformer streams, which are then efficiently distilled into a unified representation by a Perceiver module. Concurrently, it models structural connectivity from diffusion MRI using a novel signed graph transformer to encode the brain’s anatomical structure. These powerful, modality-specific representations are then integrated via an adaptive fusion gate. Despite its compact design, our model consistently outperforms larger models on a diverse range of downstream benchmarks, including classification, prediction, and unsupervised network identification tasks. Furthermore, our model revealed novel insights into brain dynamics using attention maps on a unique external psilocybin neuroimaging dataset (pre- and post-administration). BrainSymphony establishes that architecturally-aware, multimodal models can surpass their larger counterparts, paving the way for more accessible and powerful research in computational neuroscience.

1 Introduction

Understanding the brain’s dynamic activity and its underlying structural architecture is a fundamental goal of neuroscience. Functional Magnetic Resonance Imaging (fMRI) captures temporally resolved signals that reflect ongoing cognitive processes, while structural connectivity, typically derived from diffusion MRI (dMRI), encodes the anatomical pathways through which these functional dynamics are shaped and constrained. Integrating these complementary modalities promises a more holistic representation of brain function. Specifically, structural connectivity provides a stable anatomical scaffold that constrains the emergence of dynamic functional patterns, and fusing this information can lead to more neurobiologically plausible models with enhanced predictive power for individual traits and clinical outcomes [1]. However, effectively integrating these distinct data types remains a significant computational and conceptual challenge.

Early approaches to this challenge often relied on handcrafted features, such as correlation-based functional connectivity matrices [2], and shallow models like general linear models (GLMs) or Independent Component Analysis (ICA) [3]. With the rise of deep learning, more expressive models like BrainNetCNN [4] and BrainGNN [5] introduced graph-based architectures for connectivity data, which were later advanced by Transformer-based models like the Brain Network Transformer (BNT) [6] to better capture long-range dependencies. While valuable, these methods often model the

brain as a static graph, losing the rich temporal information inherent in neural signals and falling short in capturing the full hierarchical and nonlinear dependencies of brain networks [7]. This limitation prompted a shift toward dynamic models, such as TAVRNN [8], which explicitly capture the time-varying nature of brain connectivity and offer a more fine-grained view of neural dynamics.

The latest evolution is the development of large-scale, self-supervised foundation models for neuroimaging. Inspired by the success of Transformers like BERT [9] and JEPA [10] in other domains, models such as BrainLM [11] and Brain-JEPA [12] have set new benchmarks by learning generalizable representations directly from fMRI time series. However, these powerful models are often characterized by large parameter counts and data requirements. Critically, most prior work has focused on either functional or structural data in isolation, while the fusion of these intrinsic neural modalities within a unified, lightweight foundation model remains a significant open challenge.

In this work, we address this gap by introducing BrainSymphony, a Transformer-based multimodal framework designed to learn a unified representation from fMRI time series and structural connectivity. Our model’s architecture processes each modality with specialized components to capture its unique properties. For fMRI, three parallel streams—a Spatial Transformer, a Temporal Transformer, and a 1D-CNN—encode spatial, temporal, and local signal context, respectively. These diverse functional features are then distilled into a unified embedding by a Perceiver module. In parallel, a novel self-supervised Signed Graph Transformer models the structural connectome, preserving crucial information about edge weight, sign, and directionality. Finally, these modality-specific representations are integrated via an adaptive fusion gate, producing powerful embeddings that generalize to a wide range of downstream tasks.

Our contributions are threefold: (1) We propose a flexible, modular, and lightweight architecture that effectively integrates structural and functional brain data. (2) We introduce a self-supervised Signed Graph Transformer capable of modeling weighted, directed, and signed structural brain networks. (3) We demonstrate through extensive experiments that our fused multimodal representations significantly enhance performance on downstream tasks and support model interpretability. We validate BrainSymphony by pretraining it on the Human Connectome Project (HCP) dataset and evaluating its generalization on held-out data from HCP-Aging. Furthermore, the model’s interpretability is exemplified through its application to a unique external psilocybin neuroimaging dataset (pre- and post-administration), where attention maps illuminate drug-induced brain state alterations. Our results show that BrainSymphony not only achieves high performance in neuro-behavioral prediction but also offers a pathway toward more robust and clinically meaningful brain models.

2 Methods and Materials

In this section, we introduce *BrainSymphony*, a multimodal representation learning framework that integrates dynamic brain activity and structural organization into a unified latent space. Our model is composed of three key components: (1) a **Spatio-Temporal Transformer**, which encodes fMRI time series by modeling both intra- and inter-regional temporal dependencies; (2) a **Self-Supervised Signed Graph Transformer**, which learns structure-aware node representations from the anatomical connectome by incorporating edge polarity and directionality; and (3) a **Fusion Module**, which aligns and combines the latent embeddings from both modalities to produce joint ROI-level representations suitable for downstream tasks such as classification, regression, and decoding. Figure 1 illustrates the comprehensive architecture of BrainSymphony, detailing its various components.

2.1 Spatio-Temporal Transformer Framework for fMRI Representation Learning

We propose a Spatio-Temporal Transformer framework that learns distributed, biologically grounded representations from fMRI recordings. To address the high dimensionality and complex spatiotemporal dependencies inherent in brain activity, our model factorizes the representation learning process into three complementary encoding modules. The Spatial Transformer treats each region of interest (ROI) as a token and captures its anatomical identity and functional interactions across time by reconstructing masked regional signals. The Temporal Transformer treats each time point as a token and models the global temporal dependencies of brain-wide activity using sinusoidal positional priors. In parallel, a Context Extractor based on 1D convolutional filters (1D-CNN) encodes local temporal dynamics by learning contextualized features for each (ROI, time) pair.

To fuse these multi-scale representations into a coherent subject-level embedding, we adopt a Perceiver IO-style decoder. This module combines the ROI-wise embeddings from the Spatial Transformer, time-step embeddings from the Temporal Transformer, and the local spatiotemporal context vectors into unified latent tokens. Instead of applying attention directly over the entire set of $R \times T$ tokens—which is computationally prohibitive—we use a fixed set of R learnable latent vectors, each responsible for reconstructing the temporal activity of a specific ROI. These latents query the fused token space via cross-attention, enabling scalable and efficient integration of full spatiotemporal information.

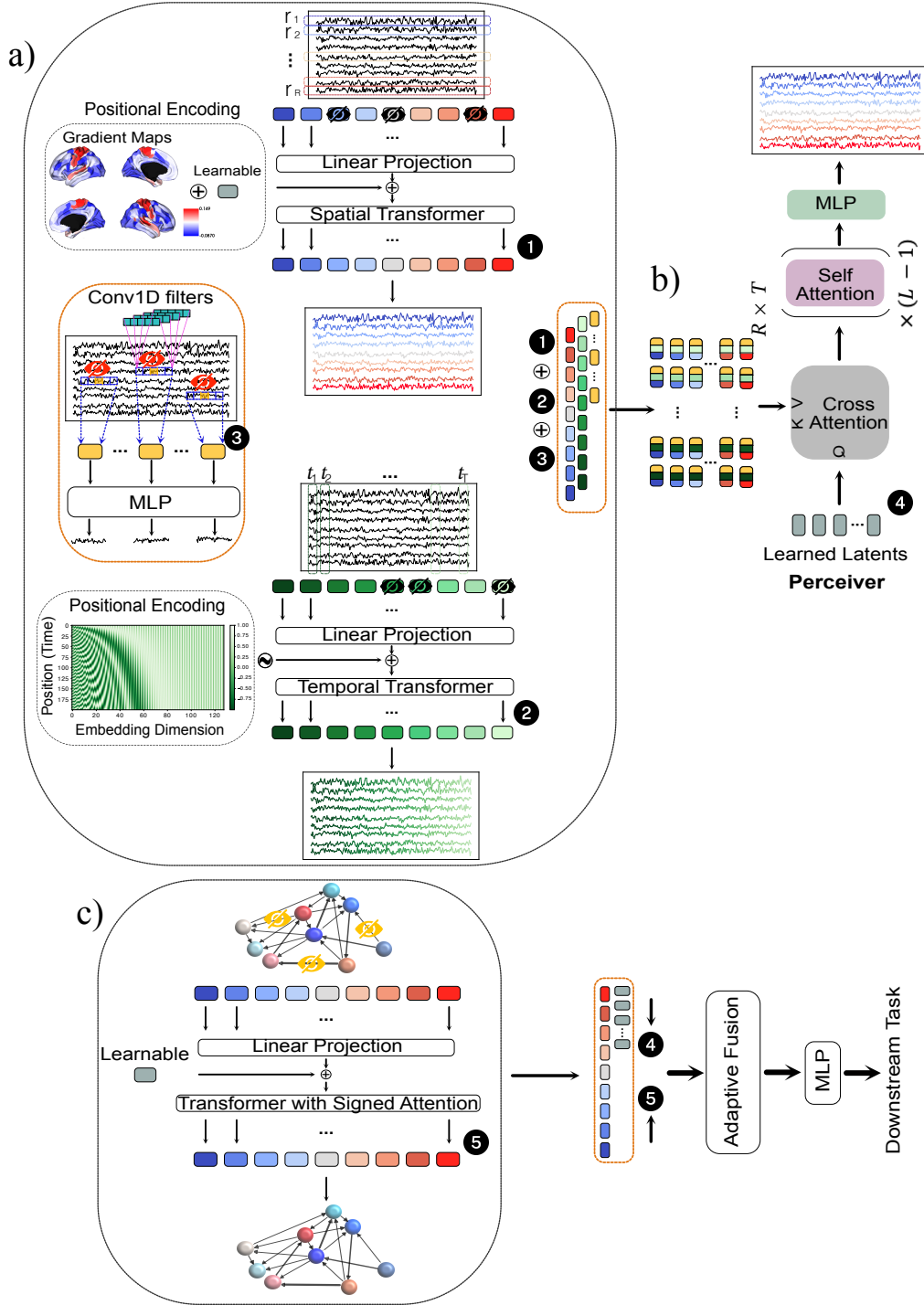


Figure 1: The architecture of BrainSymphony. **a)** Three parallel streams encode the fMRI time series: a Spatial Transformer captures relationships between brain regions, a Temporal Transformer models dynamics over time, and a 1D-CNN extracts local features from the signal context. **b)** The outputs from the three fMRI encoder streams are fed into a Perceiver module. This module uses cross-attention against a set of learned latents to distill the rich fMRI information into a compact, fixed-size representation. **c)** In parallel, a Transformer with Signed Attention encodes structural connectivity data derived from dMRI. Finally, the latent representations from both the fMRI (via the Perceiver) and dMRI streams are combined through an adaptive fusion mechanism and passed to an MLP for downstream tasks.

The resulting ROI-level latents can be interpreted as compact and informative subject-specific neural signatures, which are subsequently used for downstream tasks.

2.1.1 Problem Setup

Let $\mathbf{X} \in \mathbb{R}^{B \times R \times T}$ denote a batch of preprocessed fMRI signals, where B is the batch size, R is the number of regions of interest (ROIs), and T is the number of time points. Our objective is to encode both the temporal dynamics of neural activity and the spatial interactions among brain regions into latent representations $\mathbf{E}_{\text{fMRI}} \in \mathbb{R}^{B \times R \times d}$, which are optimized to reconstruct the original signal under partial observation. These representations are later used in our cross-modal fusion module and serve as subject-specific signatures for a variety of neurocognitive decoding tasks.

2.1.2 Spatial Transformer Encoder with Gradient-Informed Positional Encoding

To capture the spatial structure of fMRI data, we introduce a Spatial Transformer architecture that treats each ROI as a token and learns its contextual representation through self-attention over all regions. Given a single fMRI sample $\mathbf{X} \in \mathbb{R}^{R \times T}$, the model is trained to reconstruct the full activity of masked ROIs by leveraging information from unmasked regions. This masked modeling objective draws inspiration from masked autoencoders [13] and BERT-style pretraining [9], promoting distributed and robust spatial representations.

Tokenization and Masking. Each ROI’s time series $\mathbf{x}_r \in \mathbb{R}^T$ is projected into a latent embedding space via a learnable linear transformation:

$$\mathbf{z}_r = \mathbf{W}_{\text{embed}} \mathbf{x}_r, \quad \mathbf{W}_{\text{embed}} \in \mathbb{R}^{D \times T}.$$

To simulate partial observability, a binary mask $\mathbf{M} \in \{0, 1\}^R$ is sampled per input, masking a proportion p of ROIs. The embeddings of the masked ROIs are replaced with a learnable mask token $\mathbf{z}_{\text{mask}} \in \mathbb{R}^D$:

$$\tilde{\mathbf{z}}_r = M_r \cdot \mathbf{z}_r + (1 - M_r) \cdot \mathbf{z}_{\text{mask}}.$$

Gradient-Informed Positional Encoding. To embed biologically grounded spatial structure into ROI tokens, we introduce a hybrid positional encoding strategy that fuses two complementary components: (1) data-driven coordinates from functional connectivity gradients, and (2) shared learnable embeddings. This hybrid design allows the model to incorporate both subject-specific anatomical variability and population-level spatial priors.

The gradient-based component derives from the intrinsic geometry of functional brain networks. Specifically, we compute a low-dimensional embedding of the brain’s functional organization using *diffusion map embedding* [14], applied to a symmetric affinity matrix $\mathbf{A} \in \mathbb{R}^{R \times R}$ constructed from pairwise cosine distances between ROI-wise functional connectivity vectors. Each ROI i is described by its connectivity profile $\mathbf{c}_i \in \mathbb{R}^R$, and the affinity between ROIs i and j is defined as:

$$\mathbf{A}_{ij} = 1 - \frac{1}{\pi} \cos^{-1} \left(\frac{\mathbf{c}_i^\top \mathbf{c}_j}{\|\mathbf{c}_i\| \cdot \|\mathbf{c}_j\|} \right), \quad (1)$$

which ensures symmetry and bounded similarity in $[0, 1]$ based on functional similarity.

To construct the diffusion operator, we first compute the degree matrix $\mathbf{D} \in \mathbb{R}^{R \times R}$ with entries $\mathbf{D}_{ii} = \sum_j \mathbf{A}_{ij}$ and then form the *symmetric normalized graph Laplacian*:

$$\mathbf{L}_{\text{sym}} = \mathbf{I} - \mathbf{D}^{-1/2} \mathbf{A} \mathbf{D}^{-1/2}. \quad (2)$$

The eigendecomposition of \mathbf{L}_{sym} yields:

$$\mathbf{L}_{\text{sym}} \mathbf{U} = \mathbf{U} \mathbf{\Lambda}, \quad (3)$$

where $\mathbf{U} \in \mathbb{R}^{R \times R}$ contains the eigenvectors and $\mathbf{\Lambda}$ is a diagonal matrix of eigenvalues. We construct the gradient matrix $\mathbf{G} \in \mathbb{R}^{R \times K}$ by selecting the K nontrivial eigenvectors corresponding to the smallest non-zero eigenvalues (i.e., excluding the constant first eigenvector). The resulting \mathbf{G} provides a smooth, low-dimensional embedding that captures the intrinsic functional geometry of the brain, organizing ROIs along continuous gradients of connectivity.

Each row $\mathbf{g}_i \in \mathbb{R}^K$ of \mathbf{G} encodes the intrinsic functional position of ROI i in the brain’s latent manifold, revealing axes such as unimodal-to-transmodal organization.

However, since functional gradients are computed separately for each subject, the resulting coordinate spaces may be arbitrarily rotated or reflected across individuals due to the inherent sign and rotation ambiguity of eigendecomposition. This misalignment poses a significant challenge when gradients are used as positional encodings in a shared model, as corresponding ROIs across subjects may lie in incongruent embedding spaces. To ensure anatomical and functional

correspondence across subjects, we perform gradient alignment using a Procrustes-based approach. Specifically, we iteratively align all subject-level gradients into a common latent space by minimizing inter-subject variance through repeated orthogonal transformations. This procedure enables consistent and biologically meaningful positional encoding across the population, facilitating more effective learning and generalization in downstream tasks (Figure 2).

Although these gradients capture rich individual-level topographies, they may underrepresent invariant or abstract spatial priors. To address this, we concatenate each ROI’s gradient-derived embedding \mathbf{g}_r with a shared learnable positional token $\mathbf{p}_r^{\text{learn}}$, and project the result into the Transformer’s latent space using a fusion network:

$$\mathbf{P}_r = \text{MLP}([\mathbf{g}_r \mathbf{W}_g \parallel \mathbf{p}_r^{\text{learn}}]), \quad \text{s.t.} \quad \mathbf{P}_r \in \mathbb{R}^D, \mathbf{W}_g \in \mathbb{R}^{K \times D}.$$

This fused representation combines individualized anatomical-functional positioning with task-general positional priors, enabling the model to learn representations that are both neurobiologically meaningful and generalizable across subjects.

Importantly, gradient-informed positional encoding aligns with neuroscientific evidence showing that functional gradients reflect the brain’s hierarchical organization across sensory, cognitive, and associative systems [15, 16]. By leveraging this principle, our model embeds ROIs into a topological space where spatial attention mechanisms operate over continuous, functionally-relevant coordinates rather than arbitrary indices.

Transformer Architecture. The masked ROI embeddings $\tilde{\mathbf{z}}_r$ are enriched with their corresponding positional encodings:

$$\mathbf{z}'_r = \tilde{\mathbf{z}}_r + \mathbf{P}_r.$$

The resulting token sequence $\{\mathbf{z}'_r\}_{r=1}^R$ is passed through a stack of L Transformer layers, each consisting of multi-head self-attention and position-wise feedforward networks with residual connections and layer normalization:

$$\begin{aligned} \mathbf{h}_r^{(l+1)} &= \mathbf{h}_r^{(l)} + \text{Dropout} \left(\text{MSA} \left(\text{LN}(\mathbf{h}_r^{(l)}) \right) \right), \\ \mathbf{h}_r^{(l+1)} &= \mathbf{h}_r^{(l+1)} + \text{Dropout} \left(\text{MLP} \left(\text{LN}(\mathbf{h}_r^{(l+1)}) \right) \right), \end{aligned}$$

where $\mathbf{h}_r^{(0)} = \mathbf{z}'_r$.

Reconstruction and Objective. The final hidden states $\{\mathbf{h}_r\}_{r=1}^R$ are decoded through an MLP $\psi : \mathbb{R}^D \rightarrow \mathbb{R}^T$ to reconstruct the ROI time series:

$$\hat{\mathbf{x}}_r = \psi(\mathbf{h}_r).$$

Training is performed using a masked mean squared error (MSE) loss, computed only over masked ROIs:

$$\mathcal{L}_{\text{spatial}} = \frac{1}{\sum_r (1 - M_r)} \sum_{r=1}^R (1 - M_r) \cdot \|\hat{\mathbf{x}}_r - \mathbf{x}_r\|^2.$$

This objective encourages the model to infer missing regional dynamics using information from spatially and functionally related regions, fostering representations that reflect both local circuit-level activity and global cortical topology.

2.1.3 Temporal Transformer Encoder

To model the temporal dynamics of brain activity across cortical regions, we design a Temporal Transformer that treats each time step as a token and learns to predict masked time points using self-attention over temporal context. This module is complementary to the spatial encoder and aims to capture structured temporal dependencies, such as oscillations, delays, or cross-regional synchrony, that evolve across the fMRI sequence. By learning to infer missing time points, the model acquires rich temporal representations that reflect both global and local fluctuations in neural activity.

Tokenization and Masking. Given an fMRI sample $\mathbf{X} \in \mathbb{R}^{R \times T}$, we extract tokens along the temporal dimension. At each time step t , the ROI activation vector $\mathbf{x}_t \in \mathbb{R}^R$ is projected into a D -dimensional latent space using a shared linear transformation:

$$\mathbf{z}_t = \mathbf{W}_{\text{embed}} \mathbf{x}_t, \quad \text{with } \mathbf{W}_{\text{embed}} \in \mathbb{R}^{D \times R}.$$

To train under a masked modeling regime, we sample a binary temporal mask $\mathbf{M} \in \{0, 1\}^T$ that selects a proportion p of time steps to be masked. For masked positions, the token is replaced by a shared learnable embedding \mathbf{z}_{mask} :

$$\tilde{\mathbf{z}}_t = M_t \cdot \mathbf{z}_t + (1 - M_t) \cdot \mathbf{z}_{\text{mask}}.$$

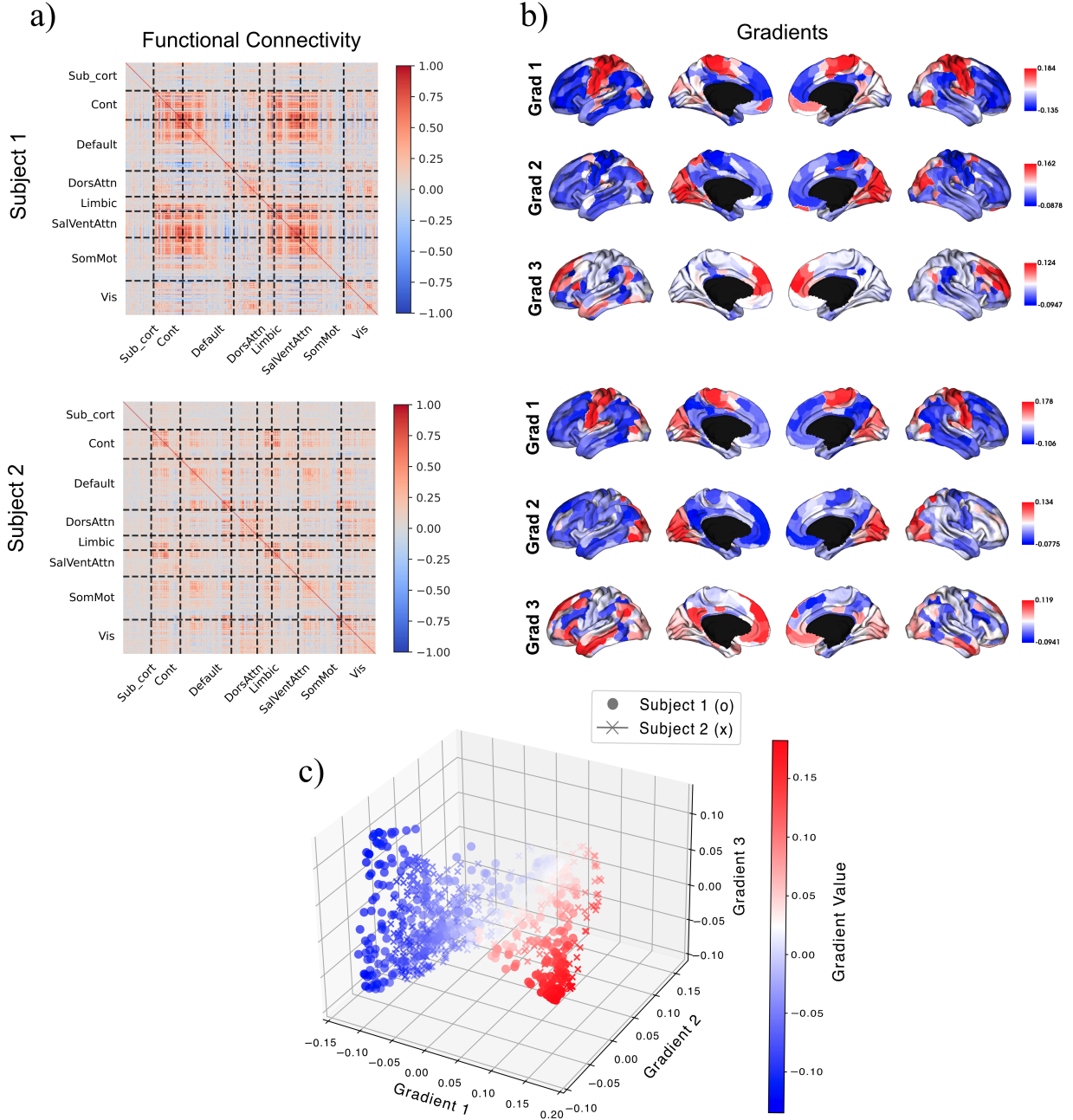


Figure 2: Gradient-Informed Positional Encoding. **a)** Subject-specific functional connectivity matrices for two example individuals, computed using Pearson correlation across ROIs. ROIs are grouped by canonical networks from Schaefer-400 and Tian-Scale III atlases (see 2.4). **b)** The first three subject-specific functional gradients derived from diffusion embedding of the affinity matrix constructed from ROI-level functional connectivity profiles. These gradients reflect the intrinsic geometry of brain organization, capturing axes such as unimodal-to-transmodal hierarchy. **c)** 3D embedding of ROI coordinates for two subjects in the shared gradient space after Procrustes alignment.

Sinusoidal Positional Encoding. To encode the temporal order of tokens, we apply a standard sinusoidal positional encoding [17]:

$$\mathbf{P}_{t,2i} = \sin\left(\frac{t}{10000^{2i/D}}\right), \quad \mathbf{P}_{t,2i+1} = \cos\left(\frac{t}{10000^{2i/D}}\right),$$

where i indexes the embedding dimensions. The encoded token is obtained by adding the positional embedding:

$$\mathbf{z}'_t = \tilde{\mathbf{z}}_t + \mathbf{P}_t.$$

This encoding allows the model to reason about the temporal structure of the signal without requiring learned positional tokens, and supports generalization across varying sequence lengths.

Transformer Architecture. The temporally ordered sequence $\{\mathbf{z}'_t\}_{t=1}^T$ is passed through a stack of L Transformer blocks, each composed of multi-head self-attention and feedforward sublayers with residual connections and layer normalization:

$$\begin{aligned} \mathbf{h}_t^{(l+1)} &= \mathbf{h}_t^{(l)} + \text{Dropout} \left(\text{MSA} \left(\text{LN}(\mathbf{h}_t^{(l)}) \right) \right), \\ \mathbf{h}_t^{(l+1)} &= \mathbf{h}_t^{(l+1)} + \text{Dropout} \left(\text{MLP} \left(\text{LN}(\mathbf{h}_t^{(l+1)}) \right) \right), \end{aligned}$$

where $\mathbf{h}_t^{(0)} = \mathbf{z}'_t$ is the initial embedded token at time step t .

Reconstruction Objective. The final temporal embeddings $\{\mathbf{h}_t\}_{t=1}^T$ are decoded via a shared MLP $\psi : \mathbb{R}^D \rightarrow \mathbb{R}^R$ to reconstruct the original ROI activation vectors:

$$\hat{\mathbf{x}}_t = \psi(\mathbf{h}_t).$$

The model is trained using a masked mean squared error loss that focuses only on the reconstruction of masked time steps:

$$\mathcal{L}_{\text{temporal}} = \frac{1}{\sum_t (1 - M_t)} \sum_{t=1}^T (1 - M_t) \cdot \|\hat{\mathbf{x}}_t - \mathbf{x}_t\|^2.$$

This objective encourages the model to capture coherent temporal dependencies across ROIs, improving its ability to model dynamic patterns such as slow cortical fluctuations, network switching, and task-evoked responses.

2.1.4 Context Extractor via 1D Convolution

While Transformers capture long-range dependencies in space and time, local temporal patterns—such as bursts, oscillations, or rapid transitions—are critical features of fMRI dynamics that can be missed by global attention mechanisms. To address this, we incorporate a convolutional context extractor that operates independently on each region’s temporal signal, allowing the model to learn fine-grained temporal structure using local filters. This module provides a complementary inductive bias by enforcing temporal locality and translation equivariance, both biologically relevant properties in cortical signal processing.

Given an fMRI sample $\mathbf{X} \in \mathbb{R}^{R \times T}$, the goal is to learn a feature representation for each (r, t) pair—i.e., each time point in each ROI—using 1D temporal convolution.

Masking Strategy. To enable self-supervised learning, we randomly mask a proportion p of the (r, t) entries. Let $\mathbf{M} \in \{0, 1\}^{R \times T}$ denote the binary mask matrix, where $M_{r,t} = 0$ indicates a masked entry. For each masked position, we replace the true value with a shared learnable scalar λ :

$$\tilde{x}_{r,t} = \begin{cases} x_{r,t}, & \text{if } M_{r,t} = 1, \\ \lambda, & \text{if } M_{r,t} = 0. \end{cases}$$

This approach preserves the input dimensionality and allows the model to distinguish masked positions from observed ones.

Local Temporal Encoding. Each masked time series $\tilde{\mathbf{x}}_r \in \mathbb{R}^T$ for ROI r is passed through a 1D convolutional encoder to extract a sequence of contextualized features:

$$\mathbf{f}_r = \text{Conv1D}_{\theta}(\tilde{\mathbf{x}}_r), \quad \mathbf{f}_r \in \mathbb{R}^{T \times D},$$

where D is the number of output channels. The convolution uses a kernel size of 5 with symmetric zero-padding to maintain the original temporal length. This architecture enables the model to attend to localized temporal neighborhoods (e.g., a window of 5 time points), capturing transient dynamics characteristic of neural signals.

Decoding and Reconstruction. For each time point t in ROI r , the corresponding feature vector $\mathbf{f}_{r,t} \in \mathbb{R}^D$ is decoded using a multi-layer perceptron (MLP) to reconstruct the original scalar value:

$$\hat{x}_{r,t} = \phi(\mathbf{f}_{r,t}), \quad \phi : \mathbb{R}^D \rightarrow \mathbb{R}.$$

Masked Reconstruction Loss. The model is trained using a masked mean squared error (MSE) loss, computed only over the masked entries:

$$\mathcal{L}_{\text{conv}} = \frac{1}{\sum_{r,t}(1 - M_{r,t})} \sum_{r=1}^R \sum_{t=1}^T (1 - M_{r,t}) \cdot (\hat{x}_{r,t} - x_{r,t})^2.$$

This objective encourages the encoder to learn temporally coherent representations that are predictive of local dynamics while remaining agnostic to unmasked positions.

2.1.5 Perceiver-Based Fusion and Reconstruction

To unify the rich, disentangled information extracted by the spatial, temporal, and contextual modules, we introduce a fusion mechanism inspired by Perceiver IO [18]. The key insight is that each ROI-time pair (r, t) carries a unique semantic meaning derived from (i) the identity of the ROI (captured via spatial embeddings), (ii) the dynamics at that time point (temporal embeddings), and (iii) local activity patterns around that point (contextual features). Rather than process the full $R \times T$ sequence of fused tokens directly—which would be computationally prohibitive—we adopt the efficient cross-attention scheme of Perceiver IO, enabling scalable modeling over high-resolution fMRI data.

Specifically, we construct a token $\mathbf{z}_{r,t}$ for every (r, t) pair by fusing three pretrained representations:

- **ROI embeddings** $\mathbf{E}^{\text{ROI}} \in \mathbb{R}^{R \times D}$ obtained from the Spatial Transformer, serving as biologically meaningful, identity-like signatures for each brain region.
- **Time embeddings** $\mathbf{E}^{\text{Time}} \in \mathbb{R}^{T \times D}$ from the Temporal Transformer, encoding shared and distinct temporal states.
- **Context features** $\mathbf{F}^{\text{Ctx}} \in \mathbb{R}^{R \times T \times d_c}$ produced by the 1D Conv-based Context Extractor, encoding fine-scale local temporal dynamics.

These embeddings are projected and concatenated into a unified token representation for each ROI-time pair:

$$\mathbf{z}_{r,t} = \text{Concat}(\mathbf{W}_r \mathbf{E}_r^{\text{ROI}}, \mathbf{W}_t \mathbf{E}_t^{\text{Time}}, \mathbf{W}_c \mathbf{F}_{r,t}^{\text{Ctx}}) \in \mathbb{R}^{d_f},$$

where $\mathbf{W}_r, \mathbf{W}_t, \mathbf{W}_c$ are learnable projection matrices that align all modalities into a common fusion space.

Latent Cross-Attention. The total number of fused tokens $\mathbf{Z} \in \mathbb{R}^{RT \times d_f}$ is typically very large and unsuitable for full attention-based modeling. To address this, we adopt the latent bottleneck architecture of Perceiver IO. A learnable array of R latent vectors $\mathbf{L} \in \mathbb{R}^{R \times d_\ell}$ —one per ROI—attends to the full set of fused tokens via a cross-attention layer:

$$\mathbf{L}' = \text{CrossAttn}(\mathbf{L}, \mathbf{Z}),$$

where each latent vector \mathbf{L}'_r aggregates information from the entire ROI-time token space relevant to reconstructing ROI r 's activity profile. These refined latents are then processed through a stack of Transformer blocks to capture interactions across ROIs in this latent space.

Reconstruction and Output. The updated latents $\{\mathbf{L}'_r\}_{r=1}^R$ are decoded into time series via an MLP:

$$\hat{\mathbf{x}}_r = \phi(\mathbf{L}'_r), \quad \phi: \mathbb{R}^{d_\ell} \rightarrow \mathbb{R}^T,$$

yielding a reconstructed output $\hat{\mathbf{X}} \in \mathbb{R}^{R \times T}$. The model is trained end-to-end to minimize the mean squared error between the reconstructed and original fMRI signals:

$$\mathcal{L}_{\text{perc}} = \frac{1}{RT} \sum_{r=1}^R \sum_{t=1}^T (\hat{x}_{r,t} - x_{r,t})^2.$$

Latent Representations for Downstream Tasks. The learned ROI-level latent vectors $\{\mathbf{L}'_r\}_{r=1}^R$ serve as high-capacity, information-rich embeddings that integrate spatial, temporal, and contextual cues. These embeddings can be directly used for downstream tasks such as subject classification, behavioral prediction, or neurological condition decoding—offering a compact, task-relevant summary of the subject's brain dynamics.

2.2 Self-Supervised Signed Graph Transformers for Structural Connectomes

To capture the anatomical organization of the brain at the network level, we introduce a self-supervised *Signed Graph Transformer* designed to encode subject-specific structural connectomes. Unlike conventional graph encoders that assume binary or symmetric adjacency structures, our model operates on fully weighted, signed, and potentially asymmetric connectivity matrices. These matrices are typically derived from tractography pipelines and reflect the directional strength and polarity of white matter connections between brain regions.

The proposed encoder learns biologically meaningful node embeddings by reconstructing masked edge weights in the adjacency matrix. It incorporates specialized attention mechanisms that are sensitive to edge sign and directionality, and it supports flexible positional encoding schemes that inject topological priors into the model. This allows the network to learn rich representations of individual brain graphs in a purely data-driven yet biologically grounded fashion, forming a structural embedding space that can later be fused with fMRI-derived representations for multimodal integration.

2.2.1 Problem Setup

Let $\mathbf{A}_s \in \mathbb{R}^{R \times R}$ denote the structural connectivity matrix of subject s , where R is the number of regions of interest (nodes) in the brain. Each element $\mathbf{A}_{s,ij}$ encodes the strength, direction, and sign of the anatomical connection from node i to node j . The objective is to learn node embeddings $\mathbf{H}_s \in \mathbb{R}^{R \times d}$ such that the structural relationships in \mathbf{A}_s can be accurately reconstructed from the learned latent space.

To enforce self-supervised learning, a subset of edges is randomly masked. The model is trained to predict the masked edge values from the node embeddings, using a reconstruction loss that penalizes deviations from the original values only at the masked locations. This masking strategy ensures that the encoder captures the local and global structure of the connectome without relying on explicit supervision.

2.2.2 Model Architecture

To model subject-specific structural connectomes with rich inductive biases, we propose a *Signed Graph Transformer* that operates on directed, weighted, and signed adjacency matrices. The goal is to learn node embeddings that capture the topology and polarity of anatomical brain connections through masked edge prediction.

Let $\mathbf{A} \in \mathbb{R}^{R \times R}$ denote a structural connectivity matrix with R regions of interest. The input features for each node are given by $\mathbf{X} \in \mathbb{R}^{R \times F}$ (e.g., identity features or node degree vectors). These are first projected into a hidden representation:

$$\mathbf{H}_0 = \mathbf{X}\mathbf{W}_{\text{in}} + \mathbf{P},$$

where $\mathbf{W}_{\text{in}} \in \mathbb{R}^{F \times d}$ is a learnable linear projection, and $\mathbf{P} \in \mathbb{R}^{R \times d}$ is a matrix of learnable positional embeddings, described below.

The model then applies L stacked Transformer layers to iteratively update the node representations:

$$\mathbf{H}_{\ell+1} = \text{TransformerLayer}(\mathbf{H}_\ell, \mathbf{A}), \quad \ell = 0, 1, \dots, L - 1.$$

2.2.3 Graph-Aware Multi-Head Signed Attention

Each Transformer layer employs a graph-aware attention mechanism designed to preserve the directionality and sign of connections.

For each attention head h , we compute:

$$\begin{aligned} \mathbf{Q}_h &= \mathbf{H}_\ell \mathbf{W}_h^Q, \quad \mathbf{K}_h = \mathbf{H}_\ell \mathbf{W}_h^K, \quad \mathbf{V}_h = \mathbf{H}_\ell \mathbf{W}_h^V, \\ \mathbf{S}_h &= \frac{1}{\sqrt{d_h}} \mathbf{Q}_h \mathbf{K}_h^\top, \end{aligned}$$

where $\mathbf{W}_h^Q, \mathbf{W}_h^K, \mathbf{W}_h^V \in \mathbb{R}^{d \times d_h}$ are projection matrices and d_h is the dimensionality per head.

To incorporate structural constraints, we modulate the raw attention scores using a signed and potentially asymmetric adjacency-aware weight matrix $\mathbf{W}_{\text{graph}} \in \mathbb{R}^{R \times R}$:

$$\mathbf{A}_h^{\text{mod}} = \text{sign}(\mathbf{S}_h \odot \mathbf{W}_{\text{graph}}) \cdot \text{softmax}(|\mathbf{S}_h \odot \mathbf{W}_{\text{graph}}|),$$

where \odot denotes elementwise multiplication. This formulation ensures that attention is distributed according to connectivity magnitude while preserving the sign of structural links.

The attended representations are then:

$$\mathbf{Z}_h = \mathbf{A}_h^{\text{mod}} \mathbf{V}_h.$$

All head outputs are concatenated and passed through a residual feed-forward layer:

$$\mathbf{Z} = \text{Concat}(\mathbf{Z}_1, \dots, \mathbf{Z}_H), \quad \mathbf{H}_{\ell+1} = \text{LayerNorm}(\mathbf{H}_\ell + \text{Dropout}(\mathbf{Z})).$$

2.2.4 Learnable Positional Encoding

Unlike temporal sequences where position reflects order, structural graphs require positional embeddings that encode relative identity and topology. We use learnable node-specific embeddings:

$$\mathbf{P} = [\mathbf{p}_1; \dots; \mathbf{p}_R] \in \mathbb{R}^{R \times d}, \quad \mathbf{p}_r \sim \mathcal{U}(-\varepsilon, \varepsilon),$$

where each \mathbf{p}_r is a trainable vector that is optimized alongside the model parameters. These embeddings allow the model to differentiate ROIs and inject flexible inductive priors for structural reasoning.

2.2.5 Masked Edge Reconstruction

To train the model in a self-supervised fashion, we adopt a masked edge prediction task. A random subset of edges $\mathcal{E}_{\text{mask}}$ is selected per subject, and their weights are held out from the loss calculation (but retained in the attention mechanism to preserve global graph structure).

After L Transformer layers, the final node embeddings $\mathbf{H} \in \mathbb{R}^{R \times d}$ are used to reconstruct the masked edges:

$$\hat{A}_{ij} = f_{\text{edge}}([\mathbf{h}_i; \mathbf{h}_j]),$$

where $[\cdot; \cdot]$ denotes concatenation and $f_{\text{edge}}: \mathbb{R}^{2d} \rightarrow \mathbb{R}$ is a multi-layer perceptron.

The training objective is a masked mean squared error:

$$\mathcal{L}_{\text{graph}} = \frac{1}{|\mathcal{E}_{\text{mask}}|} \sum_{(i,j) \in \mathcal{E}_{\text{mask}}} (\hat{A}_{ij} - A_{ij})^2.$$

This loss encourages the model to learn biologically grounded node embeddings that preserve the topology, polarity, and asymmetry of brain connectivity graphs.

2.3 Multimodal Fusion of fMRI and Structural Connectivity Representations

The brain’s functional and structural organization offer complementary insights into its computation. While fMRI captures the dynamic evolution of activity across regions of interest (ROIs), structural connectivity encodes the physical architecture that constrains such dynamics. Integrating these two modalities enables the model to learn representations that are both functionally expressive and anatomically grounded. This multimodal perspective is critical for characterizing individual variability, improving generalization across cognitive or clinical populations, and supporting downstream neurocognitive inference.

To achieve this, we introduce a modular fusion framework that combines the latent embeddings learned independently from fMRI and structural connectomes. The fused representations encode both the temporal activity patterns and the underlying white matter scaffolding, thereby forming richer node-level embeddings for each subject.

2.3.1 Problem Setup

Let $\mathbf{E}_{\text{fMRI}} \in \mathbb{R}^{B \times R \times d_f}$ denote the fMRI-derived embeddings for a batch of B subjects across R brain regions (ROIs), with d_f denoting the embedding dimensionality. These are the outputs of the Perceiver-based fusion module described in Section 2.1. Likewise, let $\mathbf{E}_{\text{SC}} \in \mathbb{R}^{B \times R \times d_s}$ represent the node embeddings learned from the Signed Graph Transformer operating on structural connectivity data (Section 2.2).

The objective is to integrate these two representations into a unified embedding:

$$\mathbf{E}_{\text{fused}} \in \mathbb{R}^{B \times R \times d_h},$$

where d_h is the dimensionality of the shared multimodal latent space. These fused embeddings serve as input to downstream modules for classification or regression tasks (e.g., sex classification or age prediction).

To effectively combine these two complementary modalities—which originate from distinct representational spaces and reflect different biological properties—we employ an *adaptive gating* mechanism. Unlike naive concatenation or static averaging, adaptive gating allows the model to dynamically modulate the contribution of each modality per region and per subject. This mechanism is particularly advantageous in multimodal neuroimaging, where the relative importance of functional versus structural information may vary across brain regions or cognitive conditions. By learning a soft gating signal, the model aligns embeddings from different spaces and produces a coherent joint representation.

Adaptive Gating Fusion. We define the fused embedding at each region as a convex combination of the fMRI and structural embeddings, weighted by a learned gate:

$$\mathbf{E}_{\text{fused}} = \sigma(\mathbf{W}_g[\mathbf{E}_{\text{fMRI}} \parallel \mathbf{E}_{\text{SC}}]) \odot \mathbf{E}_{\text{fMRI}} + (1 - \sigma(\cdot)) \odot \mathbf{E}_{\text{SC}}, \quad (4)$$

where $\parallel \cdot \parallel$ denotes concatenation along the feature dimension, $\sigma(\cdot)$ is the element-wise sigmoid function, and $\mathbf{W}_g \in \mathbb{R}^{2d \times d}$ is a learnable projection matrix. The gating mechanism thus learns a spatially varying attention over modalities, enabling flexible and biologically interpretable fusion.

2.4 Datasets

For self-supervised pretraining, we utilized data from two large-scale, public datasets: the **Human Connectome Project Young Adult (HCP-YA)** [19] and **HCP-Aging** [19] as well as a unique psilocybin neuroimaging dataset (**PsiConnect**) [20, 21]. The HCP-YA dataset includes resting-state fMRI (rs-fMRI) recordings from over 967 healthy participants aged 22-35. For pretraining, we also leveraged 40% of the HCP-Aging dataset, which corresponds to rs-fMRI data from 262 healthy participants aged 36–100+. Additionally, we utilized the external PsiConnect dataset, comprising fMRI data from 62 individuals scanned both before and after psilocybin administration. This unique dataset provided a valuable opportunity to investigate drug-induced alterations in brain dynamics.

The remaining 60% of the HCP-Aging dataset, consisting of 394 participants, was held-out as a test set for downstream evaluation tasks. During the fine-tuning and linear probing stages, this held-out data was partitioned into a 6:2:2 ratio for training, validation, and testing, respectively. Both the HCP-YA and HCP-Aging datasets feature multi-band acquisition with a high temporal resolution of approximately 0.72 seconds. For external validation, we additionally utilized the PsiConnect dataset, which features a temporal resolution (TR) of 0.91 seconds. On this external cohort, attention maps derived from our model were studied in an unsupervised manner to elucidate changes in brain dynamics as a result of psilocybin administration.

All fMRI data was preprocessed and parcellated into $n = 450$ regions of interest (ROIs) using Schaefer-400 [22] for cortical regions and Tian-Scale III [23] for subcortical regions. Following the Schaefer functional atlas, the brain network is partitioned into seven major functional subnetworks: control (Cont), default mode (Default), dorsal attention (DorsAttn), limbic (Limbic), salience/ventral attention (SalVenAttn), somatomotor (SomMot), and visual (Vis). Additionally, we include 50 subcortical regions defined by the Tian-Scale III parcellation, which we collectively refer to as Sub_Cort. Similar to previous works, robust scaling was implemented by subtracting the median and dividing by the interquartile range, calculated across participants for each ROI’s time series [11]. Our model’s default input size is 200 timesteps for each of the 450 ROIs (i.e., a tensor of shape 450×200).

2.5 Baselines

We benchmarked BrainSymphony against a diverse set of established and state-of-the-art models to evaluate its relative performance. The selected baselines represent a range of architectural approaches, from specialized deep learning models to large-scale foundation models:

- **BrainNetCNN:** A pioneering CNN-based model designed to apply convolutional operations directly to brain connectivity matrices [4].
- **BrainGNN:** A Graph Neural Network (GNN) that models brain regions as nodes and incorporates ROI-aware pooling mechanisms to learn from connectome data [5].
- **Brain Network Transformer (BNT):** A Transformer-based architecture specifically adapted to capture long-range dependencies within brain networks [6].
- **Vanilla Transformer (VT):** A standard Transformer architecture applied to brain data without domain-specific modifications, serving as a strong deep learning baseline.
- **BrainLM:** A large-scale foundation model that learns fMRI representations using a masked autoencoding strategy on time series data [11].
- **Brain-JEPA:** A state-of-the-art foundation model that utilizes a Joint Embedding Predictive Architecture (JEPA) to learn powerful representations by predicting masked data in a latent space [12].

3 Results

Figure 3 presents a comprehensive performance evaluation of our BrainSymphony model on the HCP-Aging dataset, assessing the impact of data modality (fMRI, dMRI-SC, and fusion) and training paradigm (linear probing vs. full

fine-tuning) on downstream task performance. The results consistently demonstrate the superiority of the fine-tuned, multimodal fusion approach across all evaluated tasks.

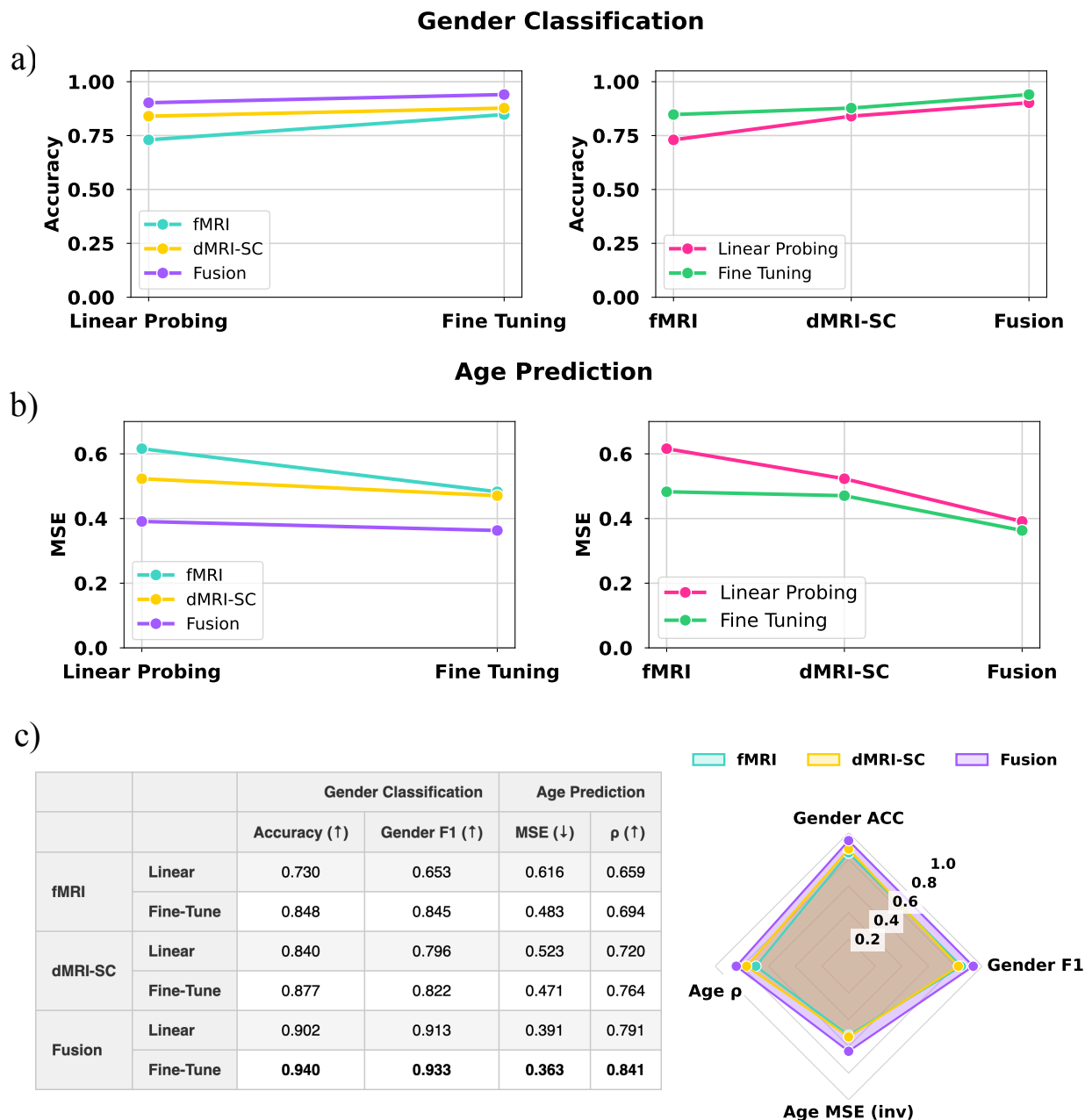


Figure 3: Performance evaluation of our BrainSymphony model on the HCP-Aging dataset. The figure compares three data input modalities (fMRI, dMRI-SC, and their fusion) across two training paradigms: linear probing and full fine-tuning. **a)** Results for the gender classification task, measured by accuracy. The fine-tuned fusion model achieves the highest accuracy. **b)** Results for the age prediction task, measured by Mean Squared Error (MSE). The fine-tuned fusion model obtains the lowest error. **c)** A detailed summary of all performance metrics across both gender classification and age prediction tasks: Accuracy, F1-Score, MSE, and correlation (ρ). The radar chart on the right provides a holistic visualization of the peak performance of the fine-tuned fusion model. For the radar chart, MSE is inverted (e.g., $1 - \text{MSE}$).

For the gender classification task (Figure 3a), fine-tuning provided a substantial performance uplift compared to linear probing for all input modalities. The fine-tuned fusion model achieved the highest performance, reaching an accuracy of 94.0% and an F1-Score of 0.933. This surpassed the performance of the fine-tuned fMRI-only (Accuracy: 84.8%) and dMRI-SC-only (Accuracy: 87.7%) models, highlighting the benefit of fusing functional and structural data.

In the age prediction task (Figure 3b), we observed a similar pattern, with the fusion model consistently yielding the lowest Mean Squared Error (MSE), where lower values indicate better performance. Specifically, the fine-tuned fusion model achieved an MSE of 0.363 and a correlation coefficient (ρ) of 0.841. The summary table and radar chart (Figure 3c) provide a detailed breakdown and holistic visualization of these peak results, confirming that the fine-tuned fusion model is the top-performing configuration.

To evaluate the performance of BrainSymphony against existing methods, we conducted a comprehensive benchmark on both gender classification and age prediction tasks. The results, summarized in Figure 3, show that our BrainSymphony models, particularly the multimodal fusion variant, consistently outperform all evaluated baseline models across the four key metrics. For gender classification (Figure 4a), the BrainSymphony models achieved the highest Accuracy and F1-Scores. Similarly, for the age prediction task (Figure 4b), the fusion model yielded the lowest Mean Squared Error (MSE) while achieving the highest correlation coefficient (ρ).

A key contribution of our work is achieving this state-of-the-art performance with a remarkably parameter-efficient model. As detailed in Figure 4c, the BrainSymphony (fusion) model contains only 5.6 million parameters. This is significantly more lightweight than other large-scale foundation models it outperforms, such as BrainLM (111M parameters) and Brain-JEPA (85M parameters). The radar chart provides a holistic visualization of this superior performance, demonstrating that BrainSymphony’s efficient architecture learns powerful and meaningful representations that generalize effectively across diverse tasks.

A detailed quantitative comparison of BrainSymphony against baseline models is presented in Table 1. The results show that the multimodal Brain Symphony (fusion) model achieves state-of-the-art performance, decisively outperforming all baseline models across all four metrics.

Table 1: Performance Comparison of Brain Symphony with Baseline Models on HCP-Aging

Model	Age Prediction		Gender Classification	
	MSE ↓	ρ ↑	ACC ↑	F1 ↑
BrainNetCNN	0.6314	0.5516	0.5720	0.7097
BrainGNN	0.6031	0.4820	0.6270	0.6818
BNT	0.5659	0.5837	0.6430	0.6968
Vanilla Transformer (VT)	0.6431	0.5321	0.5980	0.7258
BrainLM	0.5571	0.6318	0.6510	0.6800
Brain-JEPA	0.5226	0.4457	0.6742	0.6300
Brain Symphony (fMRI)	0.4828	0.6943	0.8475	0.8448
Brain Symphony (dMRI-SC)	0.4706	0.7643	0.8775	0.8218
Brain Symphony (fusion)	0.3630	0.8412	0.9404	0.9330

We further evaluated BrainSymphony’s ability to learn neuroscientifically meaningful representations by segmenting cortical parcels into intrinsic functional networks without any network-based supervision. First, 400 Shaefer cortical parcels from the HCP-Aging dataset were categorized into one of the seven canonical networks. As visualized in Figure 5, we compared the network membership predicted by our model (Figure 5a) against the ground truth (Figure 5b), and quantified the performance against other unsupervised methods.

To perform the classification, a k-NN classifier was trained on different feature types. As shown in the table in Figure 5c, using embeddings derived from BrainSymphony’s attention maps achieved a classification accuracy of 84.44%. This significantly outperformed baseline approaches that used raw parcel time series data (37.44%), or embeddings from a Variational Autoencoder (51.30%) and a Graph Convolutional Network (27.18%). These results demonstrate that BrainSymphony learns the brain’s functional topography from its pre-training objective alone, confirming that its attention maps contain rich information about network identity without exposure to explicit labels.

To characterize the re-organization of regional brain dynamics across varying conditions and pharmacological states in the PsiConnect dataset, we utilized BrainSymphony’s ROI-level receptive attention weights. Figure 6a illustrates Figure 6b presents BrainSymphony’s detailed brain maps of ROI-level receptive attention weights across four distinct experimental states—Rest, Meditation, Music, and Movie—for an individual reporting high levels of inclusion under Psilocybin administration. The rightmost column of Figure 6a further quantifies the difference in receptive attention

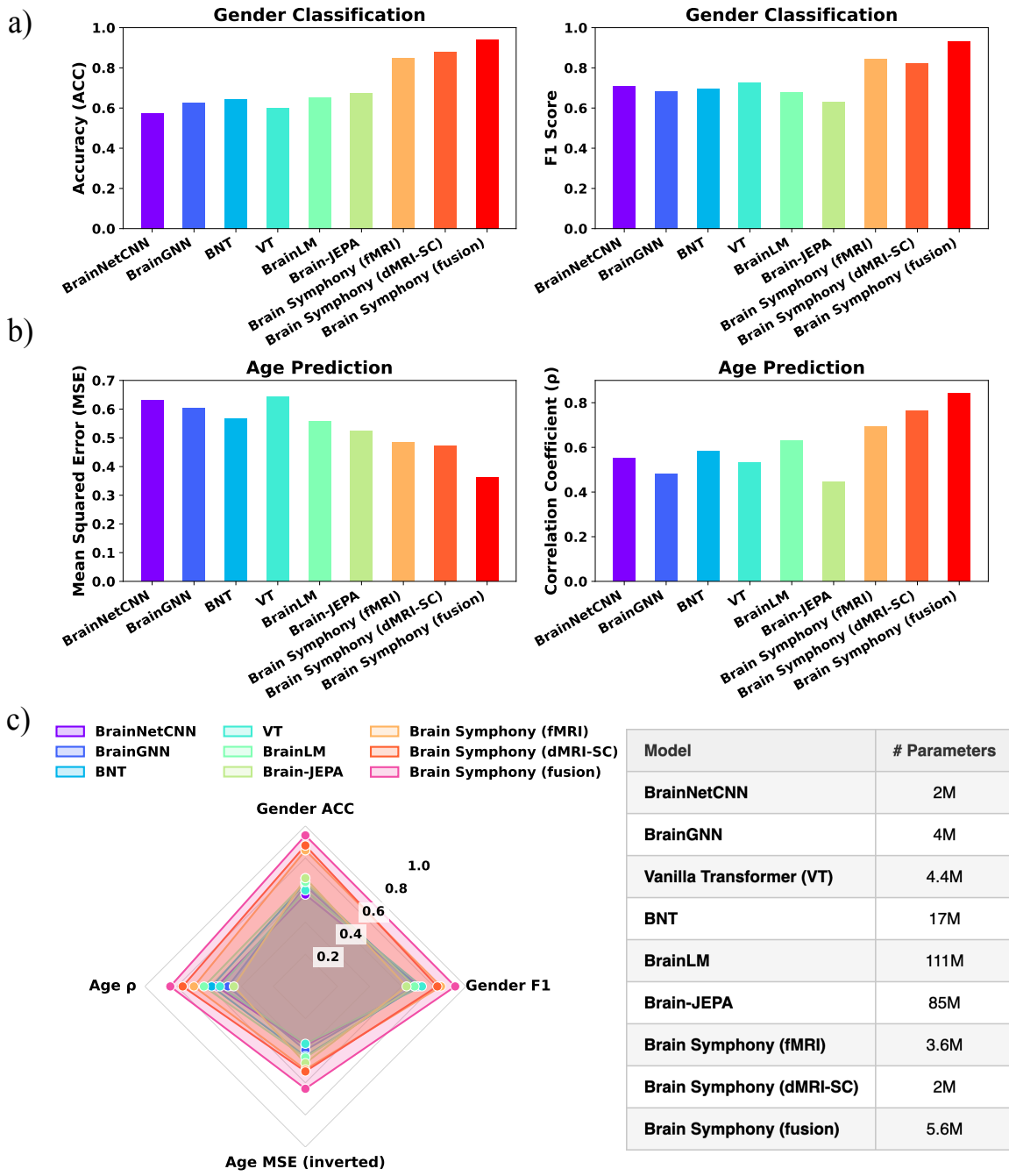


Figure 4: Comparative performance analysis of BrainSymphony against baseline models for gender classification and age prediction. **a)** Bar charts comparing model performance on gender classification, measured by Accuracy (ACC) and F1-Score. **b)** Performance on the age prediction task, measured by Mean Squared Error (MSE), and the correlation coefficient (ρ). **c)** A holistic performance summary and model complexity comparison. The radar chart visualizes the performance trade-offs across all four metrics for every model, while the table on the right details the number of parameters in all the evaluated methods. The results demonstrate that BrainSymphony (fusion) not only achieves state-of-the-art performance across all tasks but does so while being significantly more parameter-efficient than other large-scale models like BrainLM and Brain-JEPA.

weights for each of these states relative to the No-Psilocybin Rest condition. This visualization directly demonstrates

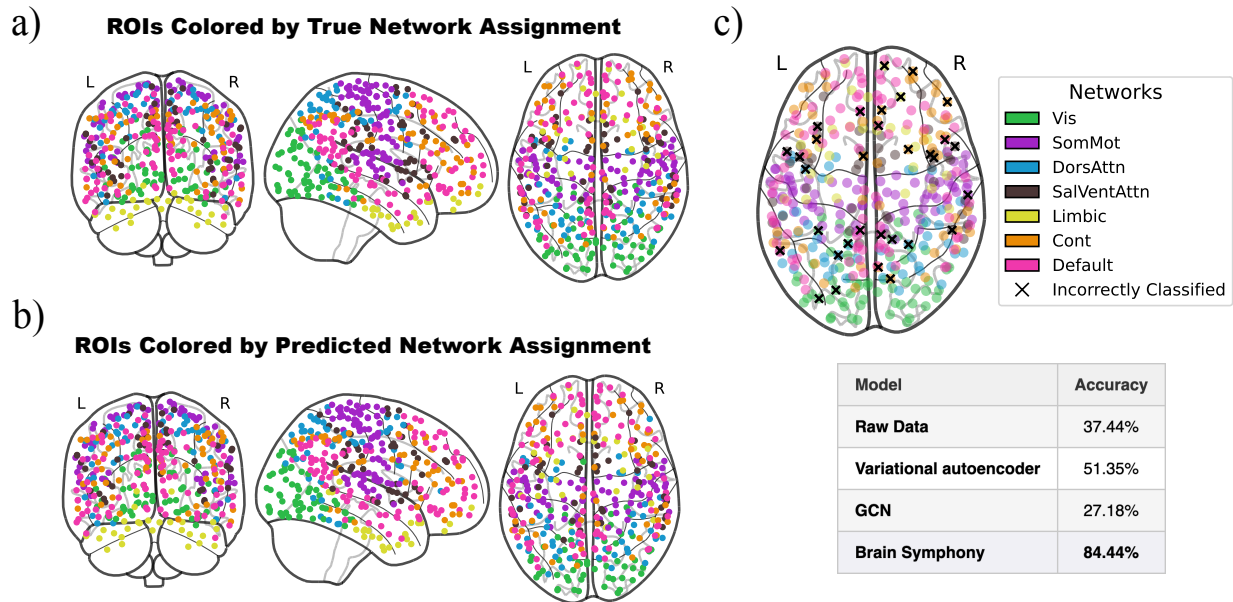


Figure 5: Unsupervised identification of functional brain networks using attention maps learned by BrainSymphony’s perceiver component. The goal is to classify 400 cortical parcels from the Schaefer atlas into one of seven canonical functional networks. **a)** The ground truth mapping of the parcels to their true functional networks, shown for visual comparison. **b)** Network assignments predicted by a k-NN classifier trained on BrainSymphony’s attention maps. **c)** A summary of classification performance. The top axial view highlights the specific ROIs incorrectly classified by our method. The table below provides a quantitative comparison of accuracy against baseline methods that use raw data or embeddings from a Graph Convolutional Network (GCN) and a Variational Autoencoder (VAE). BrainSymphony achieves the highest accuracy, demonstrating the superior quality of its learned representations for this task.

how different naturalistic contexts, such as meditation or exposure to music and movies, modulate regional attention patterns.

Figure 6b presents the corresponding receptive attention weights for the same four experimental states under the Psilocybin condition. Interestingly, a consistent increase in received attention within visual regions was observed across all four conditions following psilocybin administration. Furthermore, a striking observation from the Psilocybin conditions (the main brain maps in Figure 6b) is the increased similarity in attention patterns across the four experimental states, suggesting that the drug effect may reduce the context-dependent differences seen in the No-Psilocybin conditions (Figure 6a). Critically, the rightmost column in Figure 6(b) shows the difference in receptive attention weights for each Psilocybin state, also relative to the No-Psilocybin Rest baseline. Comparing these "Rest Diff" columns across Figure 6a and b directly highlights the distinct impact of psilocybin on the attention profiles of individual brain regions within each context. BrainSymphony’s ability to precisely delineate these complex, state- and drug-dependent shifts in receptive attention provides valuable, interpretable insights into the neurobiological underpinnings of altered consciousness and brain function.

Finally, to validate that BrainSymphony learned high-fidelity representations of brain activity, we visualized its signal reconstruction performance on held-out test data (Figure 7). The model closely reconstructs (a) the spatial activity patterns across all ROIs at individual time points, (b) the full temporal dynamics of specific ROIs over time, and (c) the structural connectivity map derived from dMRI signals between ROIs—highlighting the quality and robustness of its unsupervised learning.

Beyond quantitative performance, understanding the internal mechanisms of the BrainSymphony model is key to interpreting its capabilities. 8 illustrates the learned attention maps from core model components. These heatmaps display the average pairwise attention weights between 450 brain regions, sorted by 8 functional networks, offering insights into the intricate relationships captured within the model.

Specifically, 8a illustrates the Spatial Transformer’s attention patterns across layers. The first layer often captures more general dependencies, showing an initial homogeneous attention map across all ROIs. As attention propagates through deeper layers, exemplified by the last layer, these patterns typically become more refined and specialized. The last

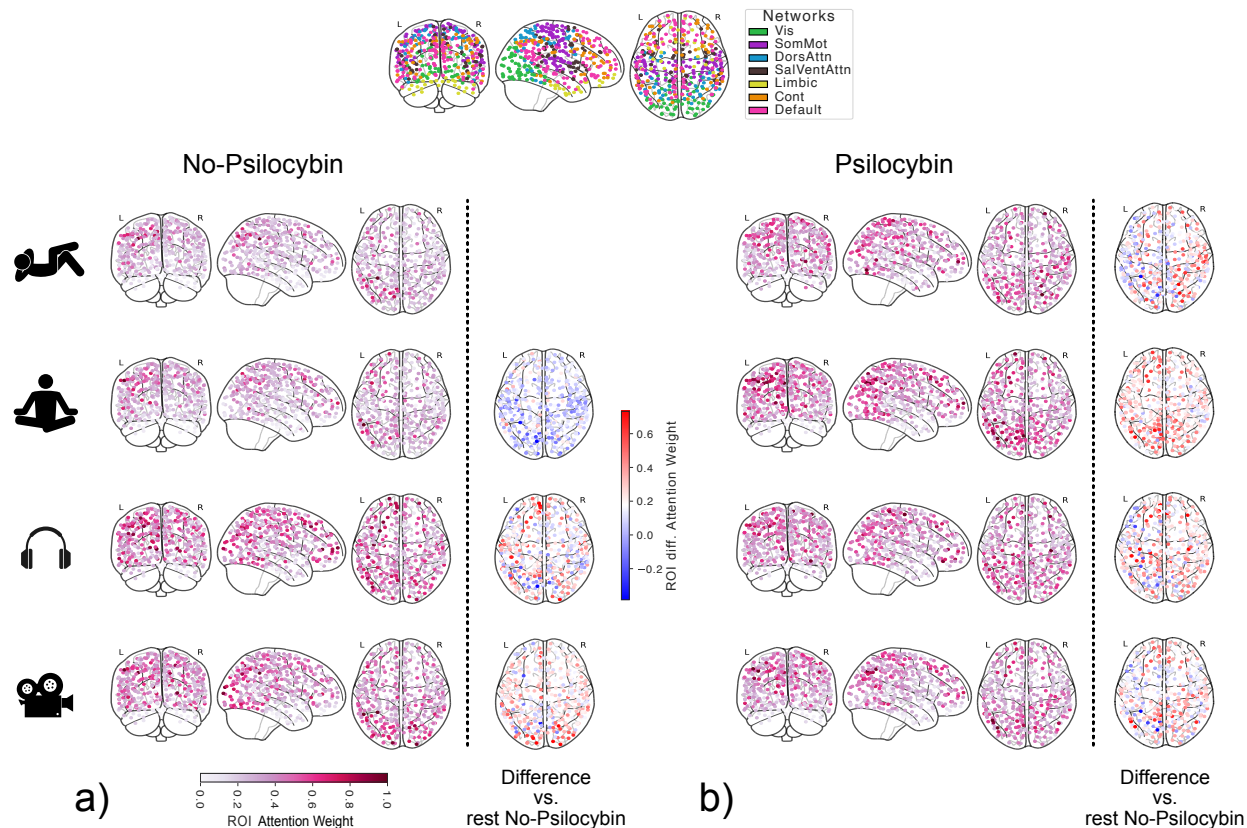


Figure 6: ROI-level receptive attention weights across conditions with and without Psilocybin. **a)** No-Psilocybin and **b)** Psilocybin conditions are shown across four experimental states: Rest, Meditation, Music, and Movie. For each state, brain maps display the receptive attention weights per ROI, defined as the sum of attention received by a given ROI from all other ROIs. The color scale reflects the normalized attention strength (bottom left). Additionally, the rightmost columns in both (a) and (b) show the difference in receptive attention weights relative to the Resting condition under No-Psilocybin, with red/blue indicating increased/decreased attention, respectively. Network labels and ROI locations follow the standard parcellation scheme shown at the top.

layer’s attention solidifies learned intra-network cohesion and clarifies more specific inter-network communication pathways, suggesting an evolution from broad to more nuanced relational understanding.

Concurrently, 8b highlights the Perceiver model’s attention maps. These patterns are particularly insightful as they reflect how the Perceiver integrates a massive spatio-temporal input (90,000 ROI-time tokens) into a distilled set of 450 ROI-specific representations. Its attention maps indicate which ROIs are deemed most relevant for integrating information across the broader context, often emphasizing a balance between maintaining network identity and fostering crucial cross-network interactions necessary for global brain processing.

Meanwhile, 8c showcases the Graph Transformer’s attention maps. By leveraging explicit graph-structured information (such as structural connectivity), this component’s attention patterns tend to exhibit strong correspondence with known brain organization. These maps can indicate not only the learned associations within networks but also how the model utilizes graph topology to identify key inter-regional relationships and hierarchical organization principles that govern brain function.

Overall, the figure demonstrates that each model component learns distinct yet complementary attention patterns. This reveals how the BrainSymphony model constructs its understanding of brain connectivity, moving from initial feature learning and intra-network processing to more refined inter-network communication and biologically informed graph-aware integration, ultimately supporting its performance in processing fMRI time series.

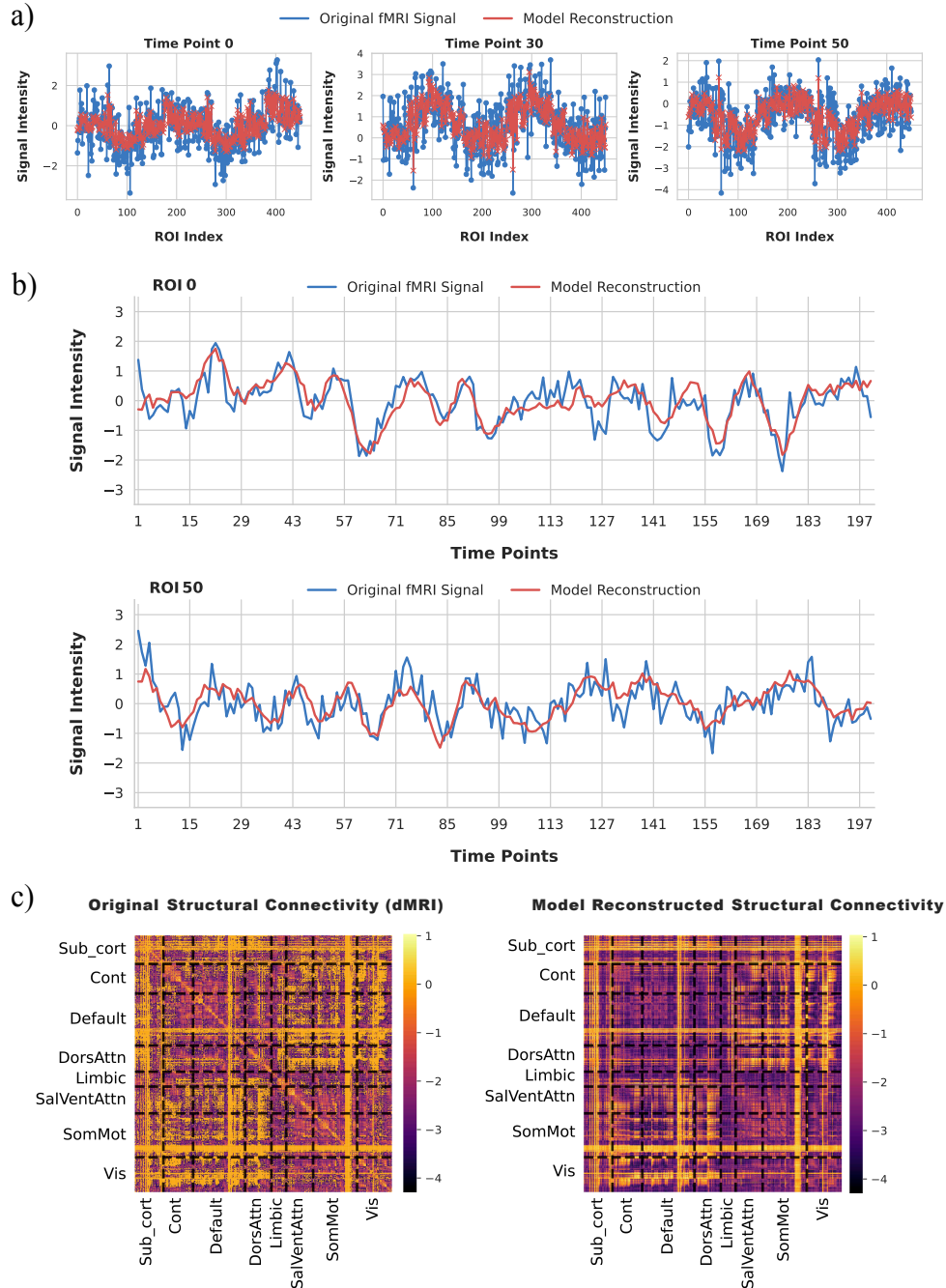


Figure 7: BrainSymphony's signal reconstruction performance on held-out test data, demonstrating the model's ability to learn spatiotemporal dynamics. **a)** Reconstruction of the spatial activity pattern across all 400 ROIs at three sample time points ($t = 0, 30,$ and 50), generated by the model's temporal transformer. **b)** Reconstruction of the full BOLD signal time series for two sample ROIs (ROI 0 and ROI 50), produced by the model's Perceiver component. In both views, the model's output (red) closely tracks the original signal (blue), indicating high-fidelity representation learning. **c)** Comparison of the original dMRI-based structural connectivity matrix (left) with the connectivity map reconstructed by BrainSymphony's signed graph transformer component (right). The reconstructed matrix preserves key topological and modular structures (e.g., within- and between-network blocks). Pairwise connections are shown between 450 ROIs, sorted and grouped by 8 functional brain networks. Network boundaries are indicated by dashed black lines.

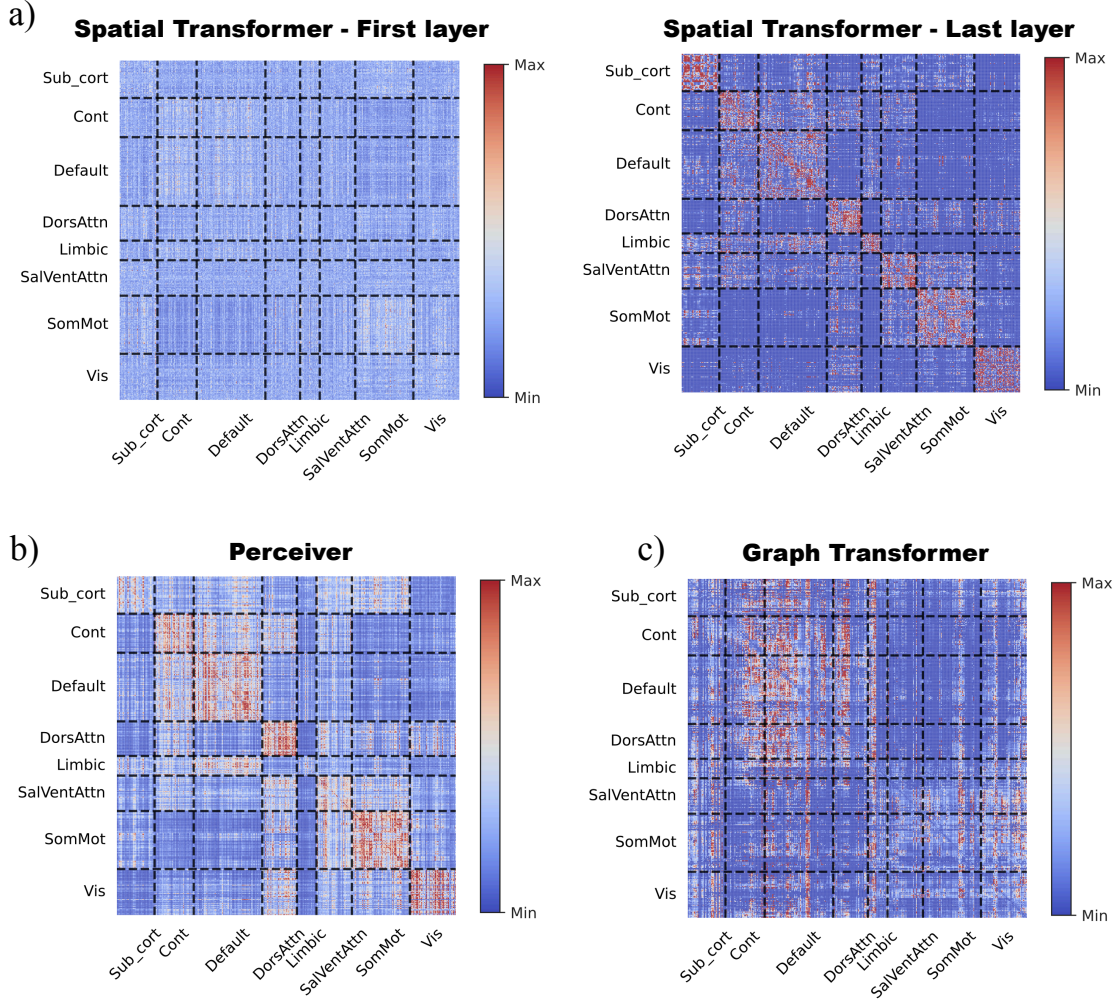


Figure 8: Attention maps from key components of the BrainSymphony model. Each heatmap displays the average pairwise attention weights between 450 ROIs, sorted and grouped by 8 functional brain networks. Network boundaries are indicated by dashed black lines. **a)** Attention within the Spatial Transformer component at the first and last layers. Stronger intra-network attention (diagonal blocks) and emergent inter-network patterns can be observed. **b)** Attention patterns from the Perceiver model. These maps highlight how the Perceiver integrates diverse input embeddings to learn ROI-specific representations, demonstrating its emphasis on intra-network coherence versus cross-network interactions. **c)** Attention patterns from the Graph Transformer, illustrating how it leverages graph-structured information to learn relationships between brain regions. These maps often reflect underlying functional connectivity and hierarchical organization within the brain. Colorbars are normalized from 'Min' to 'Max' attention values.

4 Discussion

In this work, we introduced BrainSymphony, a lightweight, multimodal foundation model that challenges the prevailing "bigger is better" paradigm in computational neuroscience. Our results demonstrate that a parameter-efficient model, trained on a smaller public dataset, can achieve and even surpass the performance of larger, data-intensive models. The success of BrainSymphony is directly attributable to its sophisticated architecture, which uses dedicated streams to capture the distinct spatial, temporal, and structural properties of brain data before integrating them through an adaptive fusion mechanism. The state-of-the-art performance on both classification (gender) and prediction (age) tasks highlights the power of this fused representation. Furthermore, the model's high accuracy in the unsupervised identification of functional networks confirms that its learned representations are not just performant but also neuroscientifically salient, as studying the learned attention maps of its components can offer powerful insights into data from different cohorts or cognitive states (e.g., task vs. rest).

An implication of this research is the potential to democratize access to high-performance neuroimaging models. By achieving superior results with significantly fewer parameters, BrainSymphony lowers the computational barrier for researchers, enabling advanced analysis without requiring massive GPU clusters. Architecturally, our work validates the use of a Perceiver module to effectively distill complex fMRI signals and demonstrates the utility of a novel signed graph transformer for capturing directed structural connectivity. A notable feature of BrainSymphony is its architectural modularity. Its components can be flexibly deployed, either individually or in concert, and our results confirm that even standalone modules achieve high predictive performance. A key limitation, however, is that our model was primarily validated on a cohort of healthy subjects. Its performance and the generalizability of its representations on more diverse clinical populations, such as in patients with neurological or psychiatric disorders, remain to be explored.

Looking forward, a promising next step is to apply BrainSymphony to clinical datasets to investigate its potential for diagnosing disease or predicting treatment outcomes. Another particularly promising avenue for future research involves leveraging the capabilities of the designed novel signed graph transformer. By extending the utilization of this component beyond structural connectivity to incorporate matrices of effective connectivity, such as those derived from Dynamic Causal Modeling (DCM), we can begin to probe the directed flow of information within brain circuits. This approach would transform BrainSymphony into a powerful framework for hypothesis testing, offering significantly greater interpretability and intuition into the neural mechanisms underlying cognition and disease. Ultimately, BrainSymphony serves as a critical step towards creating more efficient and insightful computational tools to accelerate the pace of discovery in neuroscience.

References

- [1] Olaf Sporns. *Networks of the Brain*. MIT press, 2016.
- [2] Moein Khajehnejad, Forough Habibollahi, Alon Loeffler, Brett Kagan, and Adeel Razi. On complex network dynamics of an in-vitro neuronal system during rest and gameplay. In *NeurIPS 2023 Workshop on Symmetry and Geometry in Neural Representations*, 2023.
- [3] Ewa Beldzik, Aleksandra Domagalik, Sander Daselaar, Magdalena Fafrowicz, Wojciech Froncisz, Halszka Oginska, and Tadeusz Marek. Contributive sources analysis: a measure of neural networks’ contribution to brain activations. *Neuroimage*, 76:304–312, 2013.
- [4] Jeremy Kawahara, Colin J Brown, Steven P Miller, Brian G Booth, Vann Chau, Ruth E Grunau, Jill G Zwicker, and Ghassan Hamarneh. Brainnetcnn: Convolutional neural networks for brain networks; towards predicting neurodevelopment. *NeuroImage*, 146:1038–1049, 2017.
- [5] Xiaoxiao Li, Yuan Zhou, Nicha Dvornek, Muhan Zhang, Siyuan Gao, Juntang Zhuang, Dustin Scheinost, Lawrence H Staib, Pamela Ventola, and James S Duncan. Braingnn: Interpretable brain graph neural network for fmri analysis. *Medical Image Analysis*, 74:102233, 2021.
- [6] Xuan Kan, Wei Dai, Hejie Cui, Zilong Zhang, Ying Guo, and Carl Yang. Brain network transformer. *Advances in Neural Information Processing Systems*, 35:25586–25599, 2022.
- [7] Ed Bullmore and Olaf Sporns. Complex brain networks: graph theoretical analysis of structural and functional systems. *Nature reviews neuroscience*, 10(3):186–198, 2009.
- [8] Moein Khajehnejad, Forough Habibollahi, Ahmad Khajehnejad, Brett J Kagan, and Adeel Razi. Tavrnn: Temporal attention-enhanced variational graph rnn captures neural dynamics and behavior. *arXiv preprint arXiv:2410.00665*, 2024.
- [9] Jacob Devlin, Ming-Wei Chang, Kenton Lee, and Kristina Toutanova. Bert: Pre-training of deep bidirectional transformers for language understanding. In *Proceedings of the 2019 conference of the North American chapter of the association for computational linguistics: human language technologies, volume 1 (long and short papers)*, pages 4171–4186, 2019.
- [10] Mahmoud Assran, Quentin Duval, Ishan Misra, Piotr Bojanowski, Pascal Vincent, Michael Rabbat, Yann LeCun, and Nicolas Ballas. Self-supervised learning from images with a joint-embedding predictive architecture. In *Proceedings of the IEEE/CVF Conference on Computer Vision and Pattern Recognition*, pages 15619–15629, 2023.
- [11] Josue Ortega Caro, Antonio H de O Fonseca, Christopher Averill, Syed A Rizvi, Matteo Rosati, James L Cross, Prateek Mittal, Emanuele Zappala, Daniel Levine, Rahul M Dhodapkar, et al. Brainlm: A foundation model for brain activity recordings. *bioRxiv*, pages 2023–09, 2023.
- [12] Zijian Dong, Ruilin Li, Yilei Wu, Thuan Tinh Nguyen, Joanna Chong, Fang Ji, Nathanael Tong, Christopher Chen, and Juan Helen Zhou. Brain-jepa: Brain dynamics foundation model with gradient positioning and spatiotemporal masking. *Advances in Neural Information Processing Systems*, 37:86048–86073, 2024.
- [13] Kaiming He, Xinlei Chen, Saining Xie, Yanghao Li, Piotr Dollár, and Ross Girshick. Masked autoencoders are scalable vision learners. In *Proceedings of the IEEE/CVF conference on computer vision and pattern recognition*, pages 16000–16009, 2022.
- [14] Ronald R Coifman and Stéphane Lafon. Diffusion maps. *Applied and computational harmonic analysis*, 21(1):5–30, 2006.
- [15] Daniel S Margulies, Satrajit S Ghosh, Alexandros Goulas, Marcel Falkiewicz, Julia M Huntenburg, Georg Langs, Gleb Bezdin, Simon B Eickhoff, F Xavier Castellanos, Michael Petrides, et al. Situating the default-mode network along a principal gradient of macroscale cortical organization. *Proceedings of the National Academy of Sciences*, 113(44):12574–12579, 2016.
- [16] Reinder Vos de Wael, Oualid Benkarim, Casey Paquola, Sara Lariviere, Jessica Royer, Shahin Tavakol, Ting Xu, Seok-Jun Hong, Georg Langs, Sofie Valk, et al. Brainspace: a toolbox for the analysis of macroscale gradients in neuroimaging and connectomics datasets. *Communications biology*, 3(1):103, 2020.
- [17] Ashish Vaswani, Noam Shazeer, Niki Parmar, Jakob Uszkoreit, Llion Jones, Aidan N Gomez, Łukasz Kaiser, and Illia Polosukhin. Attention is all you need. *Advances in neural information processing systems*, 30, 2017.
- [18] Andrew Jaegle, Sebastian Borgeaud, Jean-Baptiste Alayrac, Carl Doersch, Catalin Ionescu, David Ding, Skanda Koppula, Daniel Zoran, Andrew Brock, Evan Shelhamer, et al. Perceiver io: A general architecture for structured inputs & outputs. *arXiv preprint arXiv:2107.14795*, 2021.

- [19] Jennifer Stine Elam, Matthew F Glasser, Michael P Harms, Stamatios N Sotiropoulos, Jesper LR Andersson, Gregory C Burgess, Sandra W Curtiss, Robert Oostenveld, Linda J Larson-Prior, Jan-Mathijs Schoffelen, et al. The human connectome project: a retrospective. *NeuroImage*, 244:118543, 2021.
- [20] Devon Stoliker, Leonardo Novelli, Moein Khajehnejad, Mana Biabani, Tamrin Barta, Matthew D Greaves, Martin Williams, Sidhant Chopra, Olivier Bazin, Otto Simonsson, et al. Psychedelics align brain activity with context. *bioRxiv*, pages 2025–03, 2025.
- [21] Leonardo Novelli, Devon Stoliker, Tamrin Barta, Matthew D Greaves, Sidhant Chopra, James Jackson, Jessica Kwee, Martin L Williams, and Adeel Razi. Psiconnect: A multimodal neuroimaging study of psilocybin-induced changes in brain and behaviour. *bioRxiv*, pages 2025–04, 2025.
- [22] Alexander Schaefer, Ru Kong, Evan M Gordon, Timothy O Laumann, Xi-Nian Zuo, Avram J Holmes, Simon B Eickhoff, and BT Thomas Yeo. Local-global parcellation of the human cerebral cortex from intrinsic functional connectivity mri. *Cerebral cortex*, 28(9):3095–3114, 2018.
- [23] Ye Tian, Daniel S Margulies, Michael Breakspear, and Andrew Zalesky. Topographic organization of the human subcortex unveiled with functional connectivity gradients. *Nature neuroscience*, 23(11):1421–1432, 2020.